CrossMark

ARTICLE

Uranyl peroxide nanoclusters at high-pressure

Katlyn M. Turner[a)]
Department of Geological Sciences, Stanford University, Stanford, California 94305, USA

Jennifer E.S. Szymanowski
Department of Civil & Environmental Engineering & Earth Sciences, University of Notre Dame, Notre Dame, Indiana 46556, USA

Fuxiang Zhang
Materials Science and Technology Division, Oak Ridge National Laboratory, Oak Ridge, Tennessee 37831, USA

Yu Lin
Stanford Institute for Materials and Energy Sciences, SLAC National Accelerator Laboratory, Menlo Park, California 94025, USA

Brendan T. McGrail
Department of Civil & Environmental Engineering & Earth Sciences, University of Notre Dame, Notre Dame, Indiana 46556, USA

Wendy L. Mao
Department of Geological Sciences, Stanford University, Stanford, California 94305, USA; and Stanford Institute for Materials and Energy Sciences, SLAC National Accelerator Laboratory, Menlo Park, California 94025, USA

Peter C. Burns
Department of Civil & Environmental Engineering & Earth Sciences and Department of Chemistry and Biochemistry, University of Notre Dame, Notre Dame, Indiana 46556, USA

Rodney C. Ewing
Department of Geological Sciences, Stanford University, Stanford, California 94305, USA

(Received 11 May 2017; accepted 30 June 2017)

U_{60} ($[UO_2(O_2)(OH)]_{60}^{60-}$ in water) is a uranyl peroxide nanocluster with a fullerene topology and O_h symmetry. U_{60} clusters can exist in crystalline solids or in liquids; however, little is known of their behavior at high pressures. We compressed the U_{60}-bearing material: $Li_{68}K_{12}(OH)_{20}[UO_2(O_2)(OH)]_{60}(H_2O)_{310}$ ($Fm\bar{3}$; a = 37.884 Å) in a diamond anvil cell to determine its response to increasing pressure. Three length scales and corresponding structural features contribute to the compression response: uranyl peroxide bonds (<0.5 nm), isolated single nanoclusters (2.5 nm), and the long-range periodicity of nanoclusters within the solid (>3.7 nm). $Li_{68}K_{12}(OH)_{20}[UO_2(O_2)(OH)]_{60}(H_2O)_{310}$ transformed to a tetragonal structure below 2 GPa and irreversibly amorphized between 9.6 and 13 GPa. The bulk modulus of the tetragonal U_{60}-bearing material was 25 ± 2 GPa. The pressure-induced amorphous phase contained intact U_{60} clusters, which were preserved beyond the loss of long-range periodicity. The persistence of U_{60} clusters at high pressure may have been enhanced by the interaction between U_{60} nanoclusters and the alcohol pressure medium. Once formed, U_{60} nanoclusters persist regardless of their associated long-range ordering—in crystals, amorphous solids, or solutions.

I. INTRODUCTION

Uranyl peroxide nanoclusters are the only sizable group of actinide-based polyoxometallates (POMs). They are nano-sized cage-clusters with uranyl ions, UO_2^{2+}, bridged through bidentate peroxide. The dihedral uranyl peroxide angle varies between 135 and 165°, and this curvature induces the formation of the cluster.[1–4] Dozens of nanocluster topologies exist containing from 20 to 124 uranyl metal centers in the cluster cage.[1,5–19] Uranyl peroxide nanoclusters are designated by the number of uranyl metal centers in each cluster; for example, U_{24} is a cluster with 24 uranyl metal centers.[5]

Hexavalent uranium in water forms a uranyl ion,[20] and in the presence of peroxide, uranyl peroxide nanoclusters may form.[21–23] In highly radioactive environments where spent nuclear fuel interacts with water (e.g., Fukushima Daiichi nuclear power plants where ground water is in contact with melted nuclear core), alpha radiolysis of water leads to the formation of peroxide.[21–23] Uranyl peroxide nanoclusters self assemble as metastable[23]

Contributing Editor: William J. Weber
[a)]Address all correspondence to this author.
e-mail: katlynmt@stanford.edu
DOI: 10.1557/jmr.2017.301

 © Materials Research Society 2017

https://doi.org/10.1557/jmr.2017.301 Published online by Cambridge University Press

anionic entities in aqueous solutions containing uranyl and peroxide; their charge is balanced by low-valence cations. For example, U_{60}, a fullerene cluster (O_h symmetry), has a cluster formula of: $[UO_2(O_2)(OH)]_{60}$,$^{60-}$ excluding templating counterions that are not bound to the cluster. If solutions containing U_{60} clusters and sufficient counter-cations for charge balance stand open to air, the U_{60} clusters precipitate in crystals during solvent evaporation. For example, a solution of uranyl nitrate, potassium chloride, hydrogen peroxide, and lithium hydroxide produces the U_{60}-bearing compound: $Li_{68}K_{12}(OH)_{20}[UO_2(O_2)(OH)]_{60}(H_2O)_{310}$ ($Fm\bar{3}$; a = 37.884 Å) (Fig. 1).

Uranyl peroxide nanoclusters including U_{60} can be described over three different length scales and corresponding structural features that contribute to their material properties. On a local atomic scale, U_{60} clusters consist of 60 identical uranyl-peroxide-hydroxide hexagonal bipyramids that are covalently bonded[2,3] through bent, edge-sharing interactions [Fig. 2(a)]. Clusters of U_{60} [Fig. 2(b)] consist of a network of uranyl-peroxide-hydroxide hexagonal bipyramids, and each U_{60} cluster is 2.5 nm in diameter. In solids, these clusters are nested within the long-range periodicity of a crystalline material, e.g., the isometric ($Fm\bar{3}$) $Li_{68}K_{12}(OH)_{20}[UO_2(O_2)(OH)]_{60}(H_2O)_{310}$[8] [Fig. 2(c)].

Uranyl peroxide nanoclusters exist in solids and liquids. Considerable effort has been focused on the behavior, speciation, and properties of uranyl peroxide nanoclusters in solutions. If crystals containing uranyl peroxide nanoclusters are dissolved in aqueous solutions, the clusters tend to exist as mono-dispersed molecular entities.[24] In aqueous ionic solutions, they can be directed to form aggregates or "blackberries" of clusters.[25] Cluster formation can be induced in solutions mimicking the composition of dissolved spent nuclear fuel by adding peroxide to those solutions.[26,27] Due to their relatively large size, nanoclusters can be used to separate uranium from complex solutions using molecular-weight filters or porous membranes.[26,27] In aqueous solutions, uranyl peroxide nanoclusters have notably high solubility that is several orders of magnitude higher than uranyl minerals with similar compositions.[28] In nearly all of the studies of uranyl peroxide nanoclusters to date, the nanocluster is the dominant form that persists in both solids and liquids. The medium-range (approximately 2.5 nm) ordered cluster is shown not only to persist in varied chemical environments but to be a structural backbone that does not change regardless of the chemical environment. Once formed, the clusters are remarkably persistent. Because of their unique structures, uranyl peroxide nanoclusters, like U_{60}, are particularly interesting to study, as there are several structural adjustments, at different length-scales, by which these phases can respond to high pressure, high temperature, and irradiation.

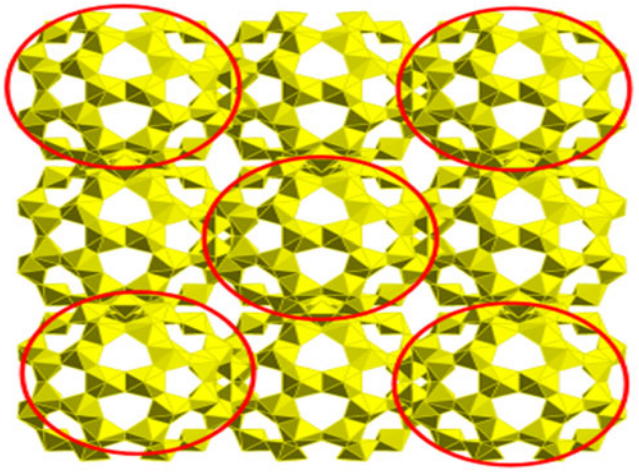


FIG. 1. One unit cell (a = 37.884 Å, from the [100] direction) of the U_{60}-bearing crystalline compound: $Li_{68}K_{12}(OH)_{20}[UO_2(O_2)(OH)]_{60}(H_2O)_{310}$ with Li, K, and H_2O omitted for clarity. Cluster molecules circled are in-plane with the page.

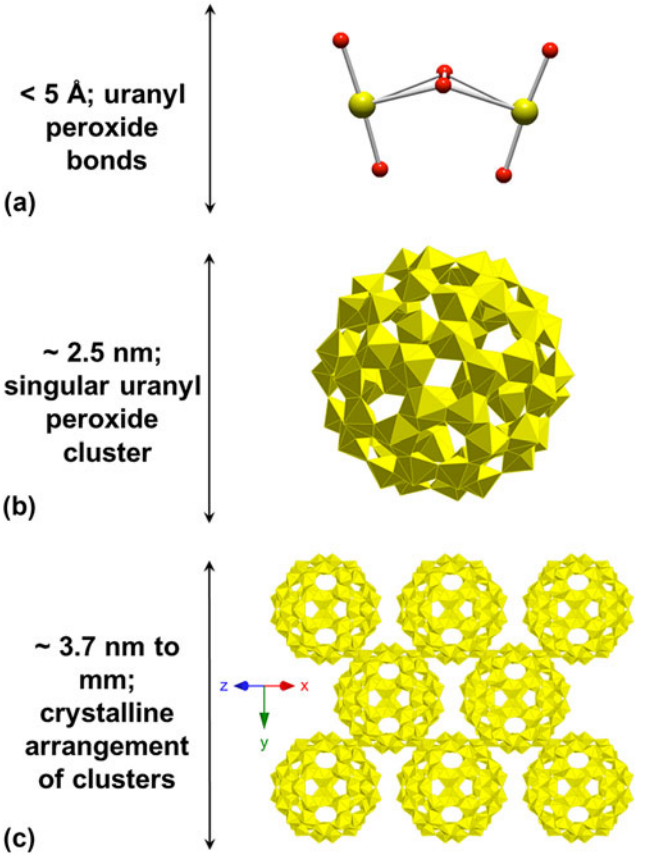


FIG. 2. Structural domains and relevant length scales in U_{60} polyoxometallates. (a) Bent uranyl peroxide bonds, giving rise to a (b) nm-sized U_{60} fullerene cluster, which packs into a (c) crystalline ($Fm\bar{3}$) arrangement extending to up to mm-sized single crystals. One unit cell (a = 37.884 Å) of $Li_{68}K_{12}(OH)_{20}[UO_2(O_2)(OH)]_{60}(H_2O)_{310}$ with Li, K, and H_2O counterions excluded for clarity.

https://doi.org/10.1557/jmr.2017.301 Published online by Cambridge University Press

Carbon fullerenes such as C_{60} and C_{70} have been the subject of high-pressure investigations,[29–37] but no actinide-based POMs have been studied at extreme pressures. In a recent study on C_{60} *m*-xylene, the high-pressure phase, which formed above 35 GPa, consisted of a hcp structure with amorphous, fragmented C_{60} clusters at each lattice site. The individual C_{60} molecules had lost their fullerene symmetry and had decomposed as a result of compression; however, the high-pressure phase still possessed long-range periodicity of the original arrangement of the clusters.

For uranyl peroxide nano-clusters, the structural response of the material to extreme environments can be investigated by observations of the long-range periodicity, the clusters themselves, and the local bonding environment of uranyl peroxides.[38–41] In this study, we report the structural evolution of the U_{60}-bearing crystalline compound: $Li_{68}K_{12}(OH)_{20}[UO_2(O_2)(OH)]_{60}(H_2O)_{310}$ at pressures up to 17.4 GPa.

II. METHODS

U_{60} clusters were synthesized, and the U_{60}-bearing crystalline compound: $Li_{68}K_{12}(OH)_{20}[UO_2(O_2)(OH)]_{60}(H_2O)_{310}$ was grown by the method of Sigmon et al.[8] Crystals of $Li_{68}K_{12}(OH)_{20}[UO_2(O_2)(OH)]_{60}(H_2O)_{310}$ were harvested from their parent solutions and loaded into diamond anvil cells (DACs) for high-pressure analysis. A symmetric Mao-Bell DAC with 300 μm culet diamonds and cubic boron nitride and tungsten carbide seats (Almax easyLab Inc., Cambridge, Massachusetts) were used to compress the sample in a stainless-steel gasket with a 130 μm diameter sample chamber. Pressure in the DAC was measured using the ruby fluorescence method.[42] A methanol:ethanol solution (4:1 by volume) was added to the stainless steel sample chamber as the pressure-transmitting medium. Methanol:ethanol was chosen over silicone oil due to its better hydrostaticity and lower reactivity with the clusters. The hydrostatic limit of methanol:ethanol (4:1) is approximately 10 GPa.[43] Gaseous pressure media (e.g., Ne, Ar, and N_2) were not used due to the possibility of diffusion into the relatively porous nanocluster topology upon compression. Additionally, there are safety-related logistical obstacles in bringing gas-loaded uranium samples in DACs to synchrotron beamlines.

The diamond anvil cell is commonly used for *in situ* studies of micron-sized materials at high pressures (>10 GPa).[44] However, materials that are highly reactive, not well crystallized, or which have complex structures are difficult to analyze using the DAC due to constraints of geometry, sample size, and available instrumentation. Researchers have made progress in recent years characterizing the structures of complex crystalline materials at high pressure in DACs with powder X-ray diffraction (XRD) and spectroscopy—e.g., hybrid perovskites[45–48] and carbon fullerenes.[29–37] Some researchers have utilized conventional single-crystal diffractometers fit with DAC mounts to study complex two-dimensional and three-dimensional structures,[29,49–54] and similar systems at synchrotron sources are under development.

Structurally complex materials may therefore require further characterization with *ex situ* and/or destructive analytical techniques to fully characterize pressure-induced effects on their structures. Even if pressure-induced structural changes are irreversible upon decompression, the amount of material recovered from a single DAC experiment is less than the typical sample requirements for mass spectroscopy experiments.

Once loaded in DACs, samples were compressed incrementally at 1–2 GPa intervals for *in situ* Raman spectroscopy and XRD measurements. For *in situ* Raman spectroscopic measurements, the maximum pressure reached was 17.4 GPa. For *in situ* XRD measurements, the maximum pressure reached was 15.6 GPa. The samples were then decompressed incrementally to ambient pressure for further *in situ* Raman and XRD measurements.

In situ high-pressure Raman spectroscopy measurements were collected at Stanford University in the Extreme Environments Laboratory using a Renishaw RM1000 Raman microscope and 514.5 nm laser (Renishaw plc, Wotton-under-Edge, United Kingdom). The laser power was kept at 3 mW to prevent laser damage to the sample and measurements were taken for 90 s at each pressure point. The Fityk program was used for spectral analysis and peak fitting.[55]

In situ high-pressure XRD measurements were collected at the Advanced Photon Source (APS) at beamline 16-BMD. The X-ray energy was 30 keV (0.4066 Å). The windows and apertures in the diamond anvil cell were covered with Kapton tape and Mylar film to enclose the sample and minimize the risk of radiation exposure if the DAC were to fail. Patterns were collected between 60 and 360 s per pressure point. The unit cell parameters were indexed using FullProf software (FullProf Suite, Institute Laue-Langevin, Grenoble, France),[56] and the pressure–volume (*P–V*) data were fit to a second-order Birch–Murnaghan equation of state (EOS)[57] using the EOSFit7GUI software (Javier Gonzalez-Platas, Matteo Alvaro, Fabrizio Nestola, and Ross Angel).[58]

Samples of compressed $Li_{68}K_{12}(OH)_{20}[UO_2(O_2)(OH)]_{60}(H_2O)_{310}$ were quenched to ambient conditions and recovered from DACs for *ex situ* analysis via Electrospray Ionization Mass Spectroscopy (ESI-MS). Seven quenched samples were necessary to obtain a high enough concentration of material for one ESI-MS measurement. For *ex situ* ESI-MS experiments, each sample was decompressed from a slightly different maximum

https://doi.org/10.1557/jmr.2017.301 Published online by Cambridge University Press

pressure, which ranged between 16 and 20 GPa. ESI-MS experiments were conducted at the University of Notre Dame at the Mass Spectrometry and Proteomics Facility. Electrospray ionization mass spectra were recorded on a Bruker microTOF-Q II (Bruker Corporation, Billerica, Massachusetts) high resolution quadrupole time of flight spectrometer with a 3200 capillary voltage, 0.4 Bar nebulizer gas, 4 L/min dry gas, and 180 °C dry gas temperature, in negative-ion mode. The samples were introduced by direct infusion and scanned over 500–4000 *m/z* with data averaged over variable time intervals.

III. RESULTS AND DISCUSSION

A. Long-range periodicity and crystallinity: *in situ* X-ray diffraction

In situ synchrotron powder XRD was used to monitor pressure-induced changes to the long-range periodicity and crystallinity of the U_{60}-bearing material: $Li_{68}K_{12}(OH)_{20}[UO_2(O_2)(OH)]_{60}(H_2O)_{310}$. At ambient conditions, this material is $Fm\bar{3}$ (a = 37.884 Å).

The large unit cell volume of $Li_{68}K_{12}(OH)_{20}[UO_2(O_2)(OH)]_{60}(H_2O)_{310}$ (a = 37.884 Å; V = 54,371 Å^3; N = 4) and the geometry of *in situ* high-pressure synchrotron powder XRD measurements diminish the available reciprocal space and the resolution of the diffraction data. The diffraction maxima overlap at 2θ greater than 4° [Fig. 3(a)]. Furthermore, $Li_{68}K_{12}(OH)_{20}[UO_2(O_2)(OH)]_{60}(H_2O)_{310}$ is sensitive in protic solvents, so powders were deliberately left with a large (5–10 μm) grain size to decrease the surface area of the sample. However, the large grain size contributed to texturing effects and preferred orientation, so peak intensities could not be refined. Peak positions were obtained and indexed [Fig. 3(b)] based on the U_{60}-bearing material published by Sigmon et al.[8] The resolution of the *in situ* data is diminished compared with an ideal powder diffraction pattern for $Li_{68}K_{12}(OH)_{20}[UO_2(O_2)(OH)]_{60}(H_2O)_{310}$ (Fig. S1), which is likely due to the sensitivity of the material in protic solvents and in air.

At 2.7 GPa, the (220) peak is broad and shows a developing shoulder [Fig. 3(b)]. At 4.4 GPa, the XRD pattern for the U_{60}-bearing material has changed, with the (022) peak of the cubic phase split, consistent with a transformation to a tetragonal structure [Fig. 3(b)]. From 4.4 to 8.6 GPa, the crystal structure of $Li_{68}K_{12}(OH)_{20}[UO_2(O_2)(OH)]_{60}(H_2O)_{310}$ retains a tetragonal structure that has not previously been observed at ambient conditions. Between 9.6 and 13.0 GPa, the diffraction features for $Li_{68}K_{12}(OH)_{20}[UO_2(O_2)(OH)]_{60}(H_2O)_{310}$ irreversibly [Fig. 3(a)] broaden, consistent with either amorphization or dissociation of the crystal into the pressure medium.

The unit cell volume of the U_{60}-bearing material decreases with pressure until 8.4 GPa. Pressure-volume data were fitted to a 2nd order Birch-Murnaghan EOS.[57] The fit (Fig. 4) shows a B_0 of 25 ± 2 GPa, and a V_0 of 53,346 Å^3 for the tetragonal material. This corresponds to

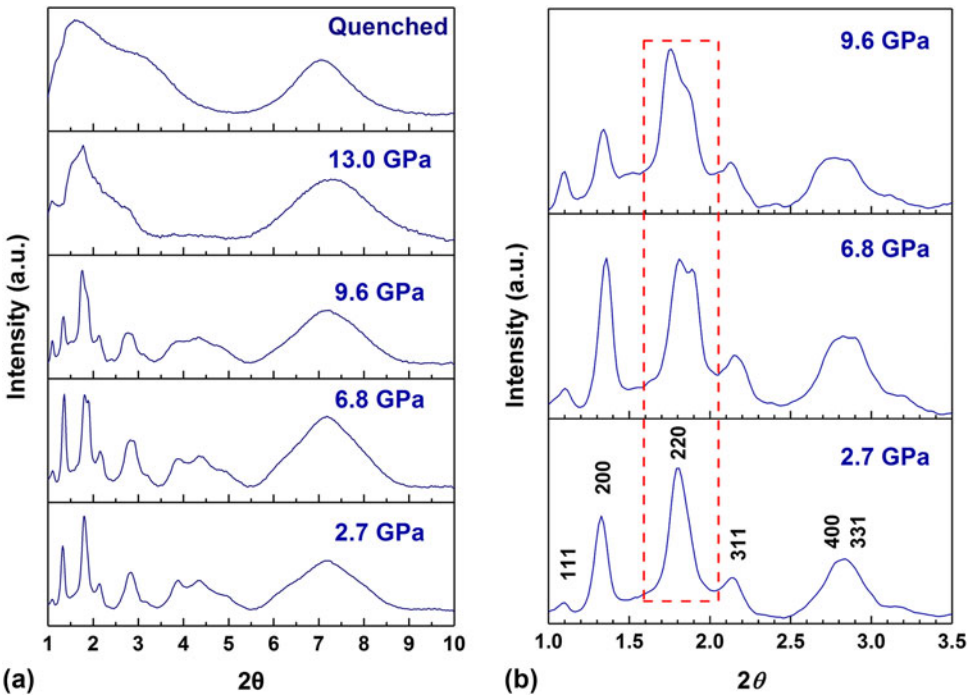


FIG. 3. (a) *In situ* synchrotron XRD (λ = 0.4066 Å) of U_{60} compound: $Li_{68}K_{12}(OH)_{20}[UO_2(O_2)(OH)]_{60}(H_2O)_{310}$ at pressures up to 13 GPa and quenched from 15.6 GPa (b) Inset from (a) showing detailed diffraction in the low 2θ region. Pressure points are identical to (a). Dashed line outlines the (022) reflection, which splits, indicating the isometric → tetragonal phase transition.

https://doi.org/10.1557/jmr.2017.301 Published online by Cambridge University Press

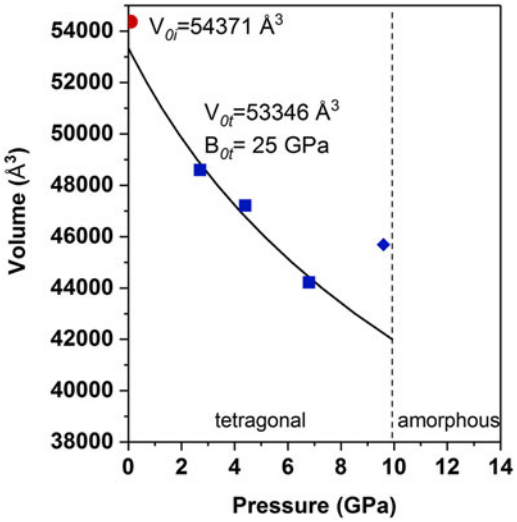


FIG. 4. Pressure–volume relationship of U_{60}-bearing compound: $Li_{68}K_{12}(OH)_{20}[UO_2(O_2)(OH)]_{60}(H_2O)_{310}$ from ambient pressure to 9.6 GPa.

a volume reduction of 1.9% as compared with the original cubic structure (V_0 = 54,371 Å^3). The volume reduction may drive the slight change in the packing and periodicity of U_{60} molecules in $Li_{68}K_{12}(OH)_{20}[UO_2(O_2)(OH)]_{60}(H_2O)_{310}$ under compression. Between 8.4 and 9.6 GPa [Figs. 3(a) and 3(b)], all peaks shift to lower 2θ, corresponding to an increase in unit cell volume (Fig. 4). This indicates that the crystalline $Li_{68}K_{12}(OH)_{20}[UO_2(O_2)(OH)]_{60}(H_2O)_{310}$ may be incorporating the alcohol pressure medium into its structure and swelling. The diffraction data indicate that the long-range periodicity of the U_{60}-bearing material is readily altered by the application of stress on the material.

Overall, the compressibility of $Li_{68}K_{12}(OH)_{20}[UO_2(O_2)(OH)]_{60}(H_2O)_{310}$ from ambient pressure to 6.8 GPa shows a volume reduction of 18.6%. This figure includes the cubic (ambient conditions) and tetragonal structures. This study is the first on an actinide polyoxometallate at high pressure, so comparisons to other materials are difficult to make. Nonetheless, the compressibility of $Li_{68}K_{12}(OH)_{20}[UO_2(O_2)(OH)]_{60}(H_2O)_{310}$ is in the range of zinc imidazolate frameworks (20–60 GPa) and slightly higher than those of hybrid perovskites (7–20 GPa).[45–48] A recent study on a two-dimensional uranyl carboxyphosphonoate compound showed a bulk modulus of 18 GPa.[40] C_{60} molecules have an identical topology to U_{60} clusters, but the bulk moduli of isometric C_{60} crystals are typically estimated to be much higher than 25 GPa.[37]

B. Short-range order: *in situ* Raman spectroscopy

Raman spectroscopy was used to complement XRD and probe the short and medium-range structural changes to U_{60} clusters ($[UO_2(O_2)(OH)]_{60}^{60-}$ excluding templating counter-cations) *in situ*. Raman spectra of uranyl peroxide nanoclusters can be used to probe the connectivity of the clusters and the curvature of the uranyl peroxide dihedral angles.[59] At ambient conditions, U_{60} clusters in the crystalline compound: $Li_{68}K_{12}(OH)_{20}[UO_2(O_2)(OH)]_{60}(H_2O)_{310}$ exhibit two Raman modes [Figs. 5(a) and 6]. One of these modes, $\nu_{O–U–O}$ at 805 cm^{-1}, corresponds to a symmetric stretch of the uranyl cation. The peak position of the symmetric stretch of the uranyl cation is significantly higher in uranyl peroxide nanoclusters than in two-dimensional uranyl compounds, where is it typically evident at approximately 700 cm^{-1}.[59] This is due to the distortion of uranyl peroxide hexagonal bipyramids in cluster compounds, relative to two-dimensional structures.

The other evident mode, $\nu_{O–O}$ at 840 cm^{-1}, corresponds to a symmetric stretch of the ⟨O–O⟩ bond from the bidentate uranyl peroxide interaction. McGrail et al. noted that this mode is present in multiple uranyl peroxide clusters and that its position correlates with the angle of curvature in the uranyl peroxide dihedral angle.[59] Together, these modes reveal the chemical species present regardless of its physical state—crystalline or amorphous.

Between 0.1 and 1 GPa, the peak positions of $\nu_{O–U–O}$ and $\nu_{O–O}$ increase by 11.1 cm^{-1}/GPa and 22.2 cm^{-1}/GPa, respectively. At 2 GPa, a new third mode is evident in the Raman spectrum (Fig. 6). This band at 890 cm^{-1} is an additional peroxide stretching mode that appears in clusters that are either in the solution, or are not rigidly templated by counter-cations in crystallographic positions.[59] The presence of this mode suggests a pressure-induced interaction between U_{60} clusters and the alcohol pressure medium. This mode is labeled as $\nu_{O–O\ sol'n}$.

At 8.6 GPa, the $\nu_{O–U–O}$ and $\nu_{O–O}$ modes overlap, and $\nu_{O–O\ sol'n}$ is evident at ~915 cm^{-1} (Fig. 6). At 17.4 GPa, above the pressure required for amorphization of the crystalline host material: $Li_{68}K_{12}(OH)_{20}[UO_2(O_2)(OH)]_{60}(H_2O)_{310}$, the Raman modes have broadened significantly, and $\nu_{O–O\ sol'n}$ has shifted to 950 cm^{-1} (Fig. 6). These Raman measurements, in combination with the XRD results, indicate that U_{60} clusters are likely still present in an amorphous solid or are in interaction with the alcohol medium. After decompression to ambient (0.1 GPa) conditions, the Raman modes of pristine U_{60} clusters in $Li_{68}K_{12}(OH)_{20}[UO_2(O_2)(OH)]_{60}(H_2O)_{310}$ could not be recovered (Fig. S2), indicating that the pressure-induced structural changes to the material are irreversible.

Figure 5(b) compares the positions of the three evident Raman modes with increasing pressure. At less than 1 GPa, the positions of $\nu_{O–U–O}$ and $\nu_{O–O}$ are around 805 cm^{-1} and 840 cm^{-1}, respectively. Above 1 GPa, the positions shift to 815 cm^{-1} and 860 cm^{-1}, respectively. At 2 GPa, the $\nu_{O–O\ sol'n}$ mode appears at 890 cm^{-1}. The slope of increase of the $\nu_{O–U–O}$ mode between 2 and 8 GPa is 2.2 cm^{-1}/GPa. The appearance of the $\nu_{O–O\ sol'n}$

https://doi.org/10.1557/jmr.2017.301 Published online by Cambridge University Press

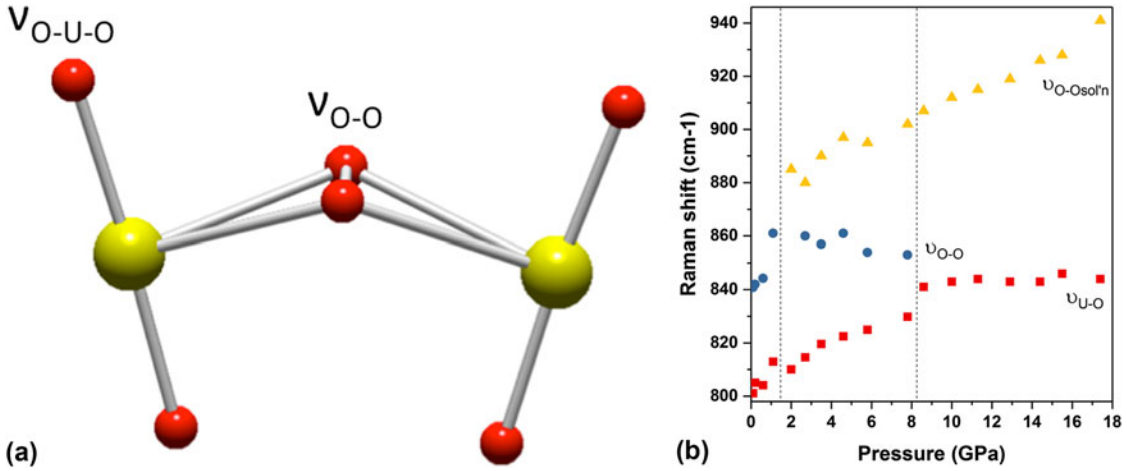


FIG. 5. (a) Ball-and-stick model of uranyl peroxide unit, showing the bent edge-sharing interaction and labeled bonds responsible for Raman active modes modes ν_{O-U-O}, ν_{O-O}, and $\nu_{O-O\ sol'n}$. (b) Plot of positions of ν_{O-U-O}, ν_{O-O}, and $\nu_{O-O\ sol'n}$ in U_{60} versus increasing pressure. Modes ν_{O-U-O} and ν_{O-O} overlap with increasing pressure beginning at the 8.6 GPa data point. Dashed lines show phase transition boundaries as indicated by *in situ* synchrotron XRD (Fig. 3).

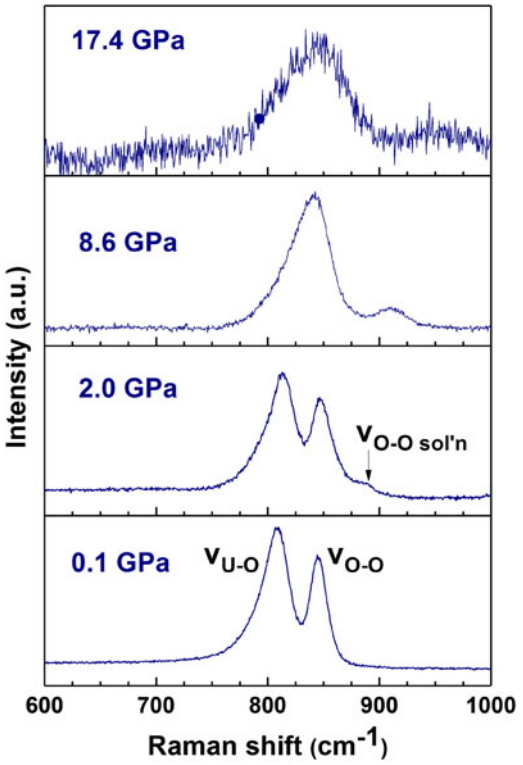


FIG. 6. Raman spectra of U_{60} in $Li_{68}K_{12}(OH)_{20}[UO_2(O_2)(OH)]_{60}(H_2O)_{310}$ at four selected pressure points. From bottom: ambient pressures, 2, 8.6, and 17.4 GPa. Modes present are the ν_{O-U-O} and ν_{O-O} modes, as well as the $\nu_{O-O\ sol'n}$ mode, which indicates the cluster interacting with the methanol:ethanol pressure medium.

mode and the discontinuity in slope in the ν_{O-U-O} mode suggests that the U_{60}-bearing material undergoes a structural change between 1 and 2 GPa. A higher Raman shift indicates a shorter uranyl bond and a more bent uranyl peroxide dihedral angle.[59] Conformational changes to the U_{60} nanocluster may drive the changes to the material's long-range periodicity and packing as is evident in the XRD analysis.

Between 2 and 8 GPa, the positions of ν_{O-U-O} and $\nu_{O-O\ sol'n}$ increase with pressure with slopes of 2.2 cm^{-1}/GPa and 3.3 cm^{-1}/GPa, respectively. The increase in peak position indicates a shorter uranyl bond and a more bent uranyl peroxide dihedral angle from which bonds are interacting with the alcohol medium and are no longer rigidly templated with counter-cations—K and Li in the $Li_{68}K_{12}(OH)_{20}[UO_2(O_2)(OH)]_{60}(H_2O)_{310}$. The ν_{O-O} mode, representative of uranyl peroxide bonds within the U_{60} nanocluster that are templated by K and Li, reaches a maximum around 860 cm^{-1}, before beginning to decrease in wavenumber between 6 and 8 GPa. This indicates a maximum in the bent angle of uranyl peroxide dihedral interactions in the $Li_{68}K_{12}(OH)_{20}[UO_2(O_2)(OH)]_{60}(H_2O)_{310}$ crystalline structure, which is achieved at approximately 5 GPa under hydrostatic conditions. McGrail et al., estimated this angle to be 115 ± 5° (versus 127 ± 5° in ambient conditions). After this point, the position of the ν_{O-O} mode decreases, indicating a relaxation of the dihedral angles, possibly caused by further interaction with the alcohol pressure medium.

Above 8 GPa, the absorption bands of ν_{O-U-O} and ν_{O-O} overlap and increase with a slope of 0.5 cm^{-1}/GPa. The position ultimately reaches a maximum around 840–845 cm^{-1} at 10 GPa, indicating a maximally compressed uranyl bond. The position of $\nu_{O-O\ sol'n}$ continues to increase at a rate of 4.7 cm^{-1}/GPa to a position as high as 940 cm^{-1} at 17.4 GPa, indicating that uranyl peroxide bonds in clusters that are not rigidly templated by counter-cations in the structure can independently undergo conformational changes.

https://doi.org/10.1557/jmr.2017.301 Published online by Cambridge University Press

C. Nano-scale order: electrospray ionization mass spectroscopy

To investigate the nature of the compressed U_{60} nanoclusters, *ex situ* ESI-MS data were collected on samples of the quenched high-pressure amorphous phase (Fig. 7). ESI-MS can be used as a fingerprinting technique to determine whether nanoclusters are still present in a material or whether nanoclusters have decomposed or changed into a different molecule. Additionally, ESI-MS is sensitive to different uranyl peroxide nanoclusters—one can distinguish between U_{60} and U_{24}, for example.[59] In Fig. 7(a), the spectra show a signal from pristine U_{60} nanoclusters dissolved in water at a concentration of 5 μM. The dominant peaks around 1900, 2100, 2400, and 2800 *m*/*z* are a fingerprint of the U_{60} clusters.[59] In Fig. 7(b), the solution from 7a was diluted in water significantly by a factor of ten to model a concentration more likely to be seen with the minuscule amount of material used in DAC experiments. The U_{60} nanocluster signal is present with a reduced intensity and peak resolution relative to 7a. Figure 7(c) shows ESI-MS spectra obtained from pressure-treated $Li_{68}K_{12}(OH)_{20}[UO_2(O_2)(OH)]_{60}(H_2O)_{310}$. Samples were taken to 16–20 GPa, compressed beyond the amorphous phase transition as indicated by XRD, and subsequently decompressed incrementally to ambient conditions. The spectra clearly indicate that the amorphous material still contains U_{60} nanoclusters that have not decomposed or changed into another type of nanocluster as a result of pressure-induced conformational changes to the cluster or by the amorphization of the surrounding structure.

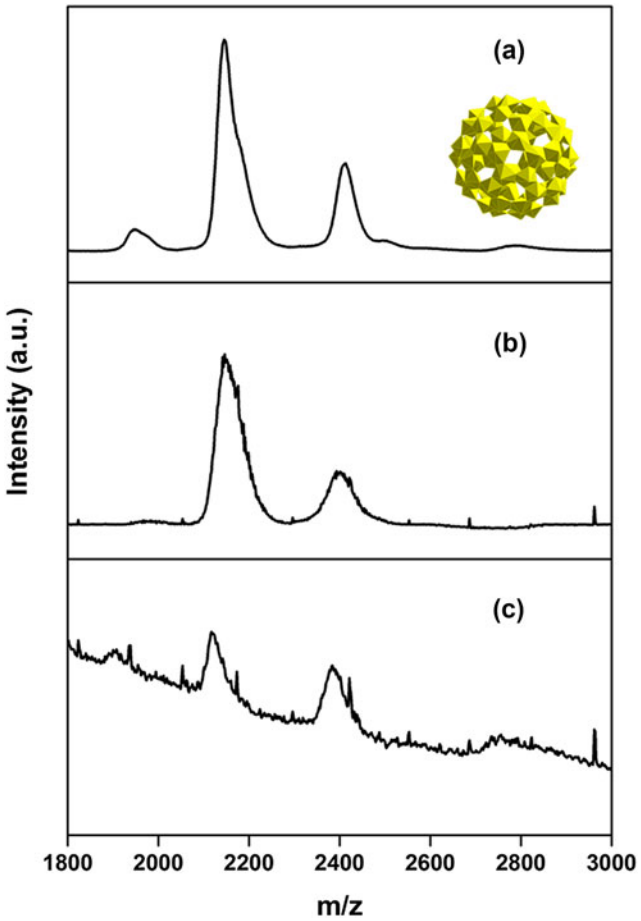


FIG. 7. ESI-MS of (a) U_{60} clusters dissolved in water, (b), ultra-low concentration of U_{60} in solution [from solution (a)], and (c) compressed U_{60} in $Li_{68}K_{12}(OH)_{20}[UO_2(O_2)(OH)]_{60}(H_2O)_{310}$ in methanol:ethanol, removed from DAC and gasket, and dissolved in water.

D. Pressure-induced changes to U_{60} clusters and $Li_{68}K_{12}(OH)_{20}[UO_2(O_2)(OH)]_{60}(H_2O)_{310}$

U_{60} clusters persist to high pressures at least several GPa higher than the amorphization pressure for the crystalline form: $Li_{68}K_{12}(OH)_{20}[UO_2(O_2)(OH)]_{60}(H_2O)_{310}$ (17.4 GPa versus 13 GPa). As the U_{60}-bearing material was subjected to pressure, the atomic and nanoscale order of the clusters and uranyl bipyramids was preserved despite the loss of the long-range periodicity.

The sequence of structural changes in the U_{60}-bearing material with increasing pressure is schematically illustrated in Fig. 8. At 2 GPa, Raman spectra indicated an interaction between U_{60} clusters and the pressure medium, as evidenced by the appearance of the $\nu_{O-O\ sol'n}$ mode. This interaction between the alcohol, nanoclusters, and crystal structure likely played a role in the subtle cubic-to-tetragonal transition (a = 36.6764(2) and c =

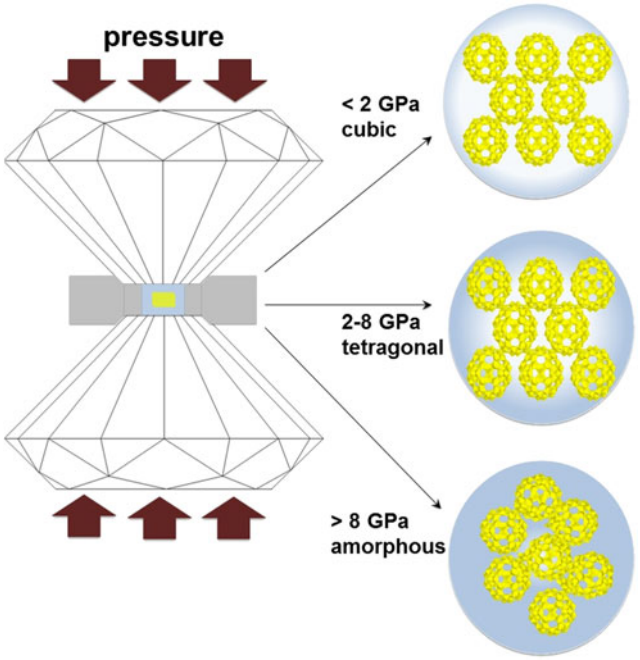


FIG. 8. The pressure-induced structural evolution of $Li_{68}K_{12}(OH)_{20}[UO_2(O_2)(OH)]_{60}(H_2O)_{310}$ in a DAC with 4:1 methanol:ethanol pressure transmitting medium. Cubic long-range structure below 2 GPa, tetragonal structure with pressure-medium interaction between 2 and 8 GPa, and amorphization + alcohol interaction above 8 GPa.

https://doi.org/10.1557/jmr.2017.301 Published online by Cambridge University Press

35.1672(4) Å). Additionally, the volume decrease—1.9% at V_0—from the cubic-to-tetragonal phase, as indicated by the equation of state, likely drove this transition.

Between 2 and 8 GPa, XRD analysis indicates an overall compression of the unit cell of $Li_{68}K_{12}(OH)_{20}[UO_2(O_2)(OH)]_{60}(H_2O)_{310}$ by 18.7%. Raman spectroscopy indicated compression of the uranyl bond and bending of the uranyl peroxide dihedral angles in U_{60} clusters. However, Raman spectroscopy also indicated a relaxation of the U_{60} cluster's dihedral angles in bonds associated with countercations—Li and K—in the structure between 6 and 8 GPa.

Between 6.8 and 9.6 GPa, XRD indicated a volume increase of the unit cell of $Li_{68}K_{12}(OH)_{20}[UO_2(O_2)(OH)]_{60}(H_2O)_{310}$. Raman spectroscopy suggests that this volume increase probably indicates swelling due to the strong interaction of the clusters with the methanol–ethanol pressure medium. Additionally, the X-ray amorphous transition between 9.6 and 13 GPa was likely driven by a strong interaction of U_{60} nanoclusters with the pressure medium, methanol:ethanol, which is nonhydrostatic above ~10 GPa. The phase transition could be due to the nonhydrostaticity of the medium. However, the determination of the specific interactions of methanol: ethanol with the $Li_{68}K_{12}(OH)_{20}[UO_2(O_2)(OH)]_{60}(H_2O)_{310}$ would be very difficult. Given that the peak position of ν_{O-O} did not increase past 8 GPa, but the peak positions of ν_{O-U-O} and $\nu_{O-O\ sol'n}$ continued to increase to the highest pressure measured (17.4 GPa), this suggests that U_{60} clusters are conformationally able to compress past 8 GPa, if no longer bound to surrounding structure, and this is facilitated by interaction with the alcohol pressure medium.

The alcohol medium causes some degradation of crystals of $Li_{68}K_{12}(OH)_{20}[UO_2(O_2)(OH)]_{60}(H_2O)_{310}$ as some U_{60} clusters are found in the solution. This was visually observed in DAC experiments because the sharp crystal faces and edges became less sharp in the presence of the methanol–ethanol mixture. Additionally, the presence of the $\nu_{O-O\ sol'n}$ mode in the Raman spectra as pressure increased indicated a cluster–alcohol interaction. At higher pressures, the U_{60} clusters continued to interact with the pressure medium, and the crystalline material became amorphous or further incorporated with the medium. Importantly, the U_{60} clusters remained intact (Fig. 7).

Nano-scale uranyl peroxide clusters are known to persist in aqueous solutions at concentrations as high as 178,000 ppm U at ambient pressure-temperature conditions.[28] Here, U_{60} nanoclusters may have interacted with the liquid medium at high pressures and may have been able to change their conformation without breaking bonds. The ESI-MS results demonstrated that rather than decomposing into smaller units, U_{60} nanoclusters existed beyond the irreversible amorphization of the crystalline phase (Fig. 7).[59]

This is the first study on uranium-bearing POMs at high pressure. Given that the U_{60} cluster's persistence at high pressure is likely influenced by its interaction with the pressure medium, similar behavior may also be exhibited in other uranyl peroxide clusters with similar chemical formulas and solubility properties. U_{60} nanoclusters may behave differently in different pressure-transmitting media: helium, argon, or nitrogen gas, for example, which would likely diffuse through the U_{60} cluster's icosahedral topology.

Uranyl peroxide nanoclusters are held together by strong covalent interactions.[2,3] This study shows that these interactions are stronger than the intermolecular forces that allow the clusters to crystallize in ambient conditions. This behavior is consistent with previous studies on uranyl peroxide nanoclusters in solids and liquids.

Very few studies on the structures of POMs at a high pressure exist. The inspiration for this study was a comparable study of a complex material with multiple ordered length-scales,[37] C_{60} *m*-xylene. C_{60} *m*-xylene is identical in topology but obviously different in chemistry from U_{60}. U_{60} nanoclusters are made up of a network of connected uranyl-peroxide-hydroxide units, whereas C_{60} involves the sp^2 bonding of a single element.[60] C_{60} *m*-xylene was studied to pressures of 40 GPa and exhibited notably different behavior at high pressure compared to the U_{60}-bearing material examined in this study. The hcp structure of C_{60} *m*-xylene was retained to 40 GPa, but at this pressure, the C_{60} molecules were fragmented.[37] A long-range ordered structure was energetically favored over the formation of an amorphous phase of intact C_{60} clusters. In the case of U_{60}, nanoscale order of the clusters was favored, as the U_{60} clusters persisted even beyond the breakdown of the long-range periodicity of the host phase. However, as in the case of U_{60}, the molecules surrounding the C_{60}, *m*-xylene, played a critical role in the ordering of the material at high pressures. The position of the *m*-xylene molecules between C_{60} cages is analogous to the presence of lithium, potassium, water, methanol, and ethanol in the $Li_{68}K_{12}(OH)_{20}[UO_2(O_2)(OH)]_{60}(H_2O)_{310}$. In the case of U_{60}, when the solvent and crystals interacted, this was a driving force for phase transitions. In the case of C_{60}, when the *m*-xylene was removed from the ordered high-pressure phase, the material amorphized within hours.[37]

IV. CONCLUSIONS

Uranyl nanoclusters, like U_{60}, persist in a variety of chemical environments both in solutions and in solids. U_{60}'s ability to exist in concentrated solutions may have allowed it to persist as a cluster at high pressure. Molecular crystals containing clusters and exhibiting long-, medium-, and short-range orders have been characterized before,[61,62] but this study on the structural response of a uranyl peroxide nanocluster to high pressures demonstrates how

https://doi.org/10.1557/jmr.2017.301 Published online by Cambridge University Press

length-scale, ordering, and chemistry can affect a material's response to extreme environments. In the case of U_{60}, the cluster, $[UO_2(O_2)(OH)]_{60}^{60-}$ excluding templating counterions, was the dominant structural feature to persist at high pressure. Although the crystalline $Li_{68}K_{12}(OH)_{20}[UO_2(O_2)(OH)]_{60}(H_2O)_{310}$ amorphized at <13 GPa, the U_{60} cluster persisted without decomposing or changing into a different phase at least to 17.4 GPa as determined by *in situ* Raman spectroscopy and to a pressure range of at least 16–20 GPa as determined by *ex situ* ESI-MS. This behavior stands in contrast to previous studies on similarly complex materials like C_{60} *m*-xylene, where a long-range ordered material with decomposed fullerenes at each lattice site was energetically favored over the formation of an amorphous phase of intact nanoclusters. The U_{60} interacted with the alcohol pressure medium, which may have enhanced the cluster's ability to compress and deform, without decomposing at high pressures.

ACKNOWLEDGMENTS

This work was supported as part of the Materials Science of Actinides, an Energy Frontier Research Center funded by the U.S. Department of Energy, Office of Science, Basic Energy Science under Award #DE-SC0001089. KMT gratefully acknowledges funding from the Stanford VPGE, DARE program. Portions of this work were performed at HPCAT (Sector 16), Advanced Photon Source (APS), Argonne National Laboratory. HPCAT operations are supported by DOE-NNSA under Award No. DE-NA0001974 and DOE-BES under Award No. DE-FG02-99ER45775, with partial instrumentation funding by NSF. The Advanced Photon Source is a U.S. Department of Energy (DOE) Office of Science User Facility operated for the DOE Office of Science by Argonne National Laboratory under Contract No. DE-AC02-06CH11357. The authors thank Dr. Changyong Park and Dr. Curtis Kenney-Benson for their help setting up these experiments.

REFERENCES

1. G. Sigmon, J. Ling, D. Unruh, L. Moore-Shay, M. Ward, B. Weaver, and P. Burns: Uranyl–peroxide interactions favor nanocluster self-assembly. *J. Am. Chem. Soc.* **131**, 16648 (2009).
2. P. Miró, S. Pierrefixe, M. Gicquel, A. Gil, and C. Bo: On the origin of the cation templated self-assembly of uranyl-peroxide nanoclusters. *J. Am. Chem. Soc.* **132**, 17787 (2010).
3. B. Vlaisavljevich, L. Gagliardi, and P. Burns: Understanding the structure and formation of uranyl peroxide nanoclusters by quantum chemical calculations. *J. Am. Chem. Soc.* **132**, 14503 (2010).
4. P. Burns and K. Hughes: Studtite, $[(UO_2)(O_2)(H_2O)_2](H_2O)_2$: The first structure of a peroxide mineral. *Am. Mineral.* **88**, 1165 (2003).
5. P. Burns, K. Kubatko, G. Sigmon, B. Fryer, J. Gagnon, M. Antonio, and L. Soderholm: Actinyl peroxide nanospheres. *Angew. Chem., Int. Ed.* **44**, 2135 (2005).
6. D. Unruh, A. Burtner, L. Pressprich, G. Sigmon, and P. Burns: Uranyl peroxide closed clusters containing topological squares. *J. Chem. Soc., Dalton Trans.* **39**, 5807 (2010).
7. T. Forbes, J. McAlpin, R. Murphy, and P. Burns: Metal–oxygen isopolyhedra assembled into fullerene topologies. *Angew. Chem., Int. Ed.* **47**, 2824 (2008).
8. G. Sigmon, D. Unruh, J. Ling, B. Weaver, M. Ward, L. Presspich, A. Simonetti, and P. Burns: Symmetry versus minimal pentagonal adjacencies in uranium-based polyoxometalate fullerene topologies. *Angew. Chem., Int. Ed.* **48**, 2737 (2009).
9. D. Unruh, J. Ling, J. Qiu, L. Pressprich, M. Baranay, M. Ward, and P. Burns: Complex nanoscale cage clusters built from uranyl polyhedra and phosphate tetrahedra. *Inorg. Chem.* **50**, 5509 (2011).
10. J. Ling, J. Qiu, J. Szymanowski, and P. Burns: Low-symmetry uranyl pyrophosphate cage clusters. *Chem.–Eur. J.* **17**, 2571 (2011).
11. J. Ling, C. Wallace, J. Szymanowski, and P. Burns: Hybrid uranium–oxalate fullerene topology cage clusters. *Angew. Chem., Int. Ed.* **49**, 7271 (2010).
12. J. Ling, M. Ozga, M. Stoffer, and P. Burns: Uranyl peroxide pyrophosphate cage clusters with oxalate and nitrate bridges. *J. Chem. Soc., Dalton Trans.* **41**, 7278 (2012).
13. J. Qiu, J. Ling, L. Jouffret, R. Thomas, J. Szymanowski, and P. Burns: Water-soluble multi-cage super tetrahedral uranyl peroxide phosphate clusters. *Chem. Sci.* **5**, 303 (2014).
14. J. Qiu, J. Ling, A. Sui, J. Szymanowski, A. Simonetti, and P. Burns: Time-resolved self-assembly of a fullerene-topology core–shell cluster containing 68 uranyl polyhedra. *J. Am. Chem. Soc.* **134**, 1810 (2012).
15. J. Ling, J. Qiu, G. Sigmon, M. Ward, J. Szymanowski, and P. Burns: Uranium pyrophosphate/methylenediphosphonate polyoxometalate cage clusters. *J. Am. Chem. Soc.* **132**, 13395 (2010).
16. J. Qiu, K. Nguyen, L. Jouffret, J. Szymanowski, and P. Burns: Time-resolved assembly of chiral uranyl peroxo cage clusters containing belts of polyhedra. *Inorg. Chem.* **52**, 337 (2013).
17. J. Ling, J. Qiu, and P. Burns: Uranyl peroxide oxalate cage and core–shell clusters containing 50 and 120 uranyl ions. *Inorg. Chem.* **51**, 2403 (2012).
18. P. Burns: Nanoscale uranium-based cage clusters inspired by uranium mineralogy. *Mineral. Mag.* **75**, 1 (2011).
19. J. Qiu and P. Burns: Clusters of actinides with oxide, peroxide or hydroxide bridges. *Chem. Rev.* **113**, 1097 (2012).
20. P. Burns, R. Ewing, and F. Hawthorne: The crystal chemistry of hexavalent uranium: Polyhedron geometries, bond-valence parameters, and polymerization of polyhedra. *Can. Mineral.* **35**, 1551 (1997).
21. P. Burns: U^{6+} minerals and inorganic compounds: Insights into an expanded structural hierarchy of crystal structures. *Can. Mineral.* **43**, 1839 (2005).
22. P. Burns, R. Ewing, and A. Navrotsky: Nuclear fuel in a reactor accident. *Science* **335**, 1184 (2012).
23. C. Armstrong, M. Nyman, T. Shvareva, G. Sigmon, P. Burns, and A. Navrotsky: Uranyl peroxide enhanced nuclear fuel corrosion in seawater. *Proc. Natl. Acad. Sci.* **109**, 1874 (2012).
24. S. Flynn, J. Szymanowski, Y. Gao, T. Liu, P. Burns, and J. Fein: Experimental measurements of U_{60} nanocluster stability in aqueous solution. *Geochim. Cosmochim. Acta* **156**, 94 (2015).
25. C. Wallace: Solution and aggregation behavior of the U_{60} nanocluster and post-detonation nuclear forensic analysis of trinitite. Ph.D. thesis, University of Notre Dame, Notre Dame, Indiana, 2013.
26. E. Wylie, K. Peruski, J. Weidman, W. Phillip, and P. Burns: Ultrafiltration of uranyl peroxide nanoclusters for the separation of uranium from aqueous solution. *ACS Appl. Mater. Interfaces.* **6**, 473 (2013).
27. E. Wylie, K. Peruski, S. Prizio, A. Bridges, T. Rudisill, D. Hobbs, W. Phillip, and P. Burns: Processing used nuclear fuel with

https://doi.org/10.1557/jmr.2017.301 Published online by Cambridge University Press

nanoscale control of uranium and ultrafiltration. *J. Nucl. Mater.* **473**, 125 (2016).
28. K. Peruski, V. Bernales, M. Dembowski, H. Lobeck, K. Pellegrini, G. Sigmon, S. Hickam, C. Wallace, J. Szymanowski, E. Balboni, L. Gagliardi, and P. Burns: Uranyl peroxide cage cluster solubility in water and the role of the electrical double layer. *Inorg. Chem.* **56**, 1333 (2017).
29. J. Patterson, S. Catledge, Y. Vohra, J. Akella, and S. Weir: Electrical and mechanical properties of C_{70} fullerene and graphite under high pressures studied using designer diamond anvils. *Phys. Rev. Lett.* **85**, 5634 (2000).
30. R. Kumar, M. Pravica, A. Cornelius, M. Nicol, M. Hu, and P. Chow: X-ray Raman scattering studies on C_{60} fullerenes and multi-walled carbon nanotubes under pressure. *Diamond Relat. Mater.* **16**, 1250 (2007).
31. U. Venkateswaran, A. Rao, E. Richter, M. Menon, A. Rinzler, R. Smalley, and P. Eklund: Probing the single-wall carbon nanotube bundle: Raman scattering under high pressure. *Phys. Rev. B: Condens. Matter Mater. Phys.* **59**, 10928 (1999).
32. E. Miller, D. Nesting, and J. Badding: Quenchable transparent phase of carbon. *Chem. Mater.* **9**, 18 (1997).
33. A. Sood, P. Teresdesai, D. Muthu, R. Sen, A. Govindaraj, and C. Rao: Pressure behaviour of single wall carbon nanotube bundles and fullerenes: A Raman study. *Phys. Status Solidi B* **215**, 393 (1999).
34. J. Patterson, Y. Vohra, S. Weir, and J. Akella: Single-wall carbon nanotubes under high pressures to 62 GPa studied using designer diamond anvils. *J. Nanosci. Nanotechnol.* **1**, 143 (2001).
35. J. Patterson, S. Catledge, Y. Vohra, J. Akella, and S. Weir: Electrical and mechanical properties of C_{70} fullerene and graphite under high pressures studied using designer diamond anvils. *Phys. Rev. Lett.* **85**, 5364 (2000).
36. Y. Lin, L. Zhang, H. Mao, P. Chow, Y. Xiao, M. Baldini, J. Shu, and W. Mao: Amorphous diamond: A high-pressure superhard carbon allotrope. *Phys. Rev. Lett.* **107**, 175504 (2011).
37. L. Wang, B. Liu, H. Li, W. Yang, Y. Ding, S. Sinogeikin, Y. Meng, Z. Liu, X. Zeng, and W. Mao: Long-range ordered carbon clusters: A crystalline material with amorphous building blocks. *Science* **337**, 825 (2012).
38. D. Wang and A. Fernandez-Martinez: Order from disorder. *Science* **337**, 812 (2012).
39. S. Elliott: Medium-range structural order in covalent amorphous solids. *Nature* **354**, 445 (1991).
40. G. Lucovsky: Specification of medium range order in amorphous materials. *J. Non-Cryst. Solids* **97**, 155 (1987).
41. L. Červinka: Medium-range ordering in non-crystalline solids. *J. Non-Cryst. Solids* **90**, 371 (1987).
42. H. Mao, P. Bell, J. Shaner, and S. Steinberg: Specific volume measurements of Cu, Mo, Pd, and Ag and calibration of the ruby R_1 fluorescence pressure gauge from 0.06 to 1 Mbar. *J. Appl. Phys.* **49**, 3276 (1978).
43. R. Angel, M. Bujak, J. Zhao, G. Gatta, and S. Jacobsen: Effective hydrostatic limits of pressure media for high-pressure crystallographic studies. *J. Appl. Crystallogr.* **40**, 26 (2007).
44. W. Bassett: Diamond anvil cell, 50th birthday. *High Pressure Res.* **29**, 163 (2009).
45. A. Jaffe, Y. Lin, W. Mao, and H. Karunadasa: Pressure-induced conductivity and yellow-to-black piezochromism in a layered Cu–Cl hybrid perovskite. *J. Am. Chem. Soc.* **137**, 1673 (2015).
46. S. Jiang, Y. Fang, R. Li, H. Xiao, J. Crowley, C. Wang, T. White, W. Goddard, Z. Wang, T. Baikie, and J. Fang: Pressure-dependent polymorphism and band-gap tuning of methylammonium lead iodide perovskite. *Angew. Chem., Int. Ed.* **55**, 6540 (2016).
47. D. Umeyama, Y. Lin, and H. Karunadasa: Red-to-black piezochromism in a compressible Pb–I–SCN layered perovskite. *Chem. Mater.* **28**, 3241 (2016).
48. A. Jaffe, Y. Lin, C. Beavers, J. Voss, W. Mao, and H. Karunadasa: High-pressure single-crystal structures of 3D lead-halide hybrid perovskites and pressure effects on their electronic and optical properties. *ACS Cent. Sci.* **2**, 201 (2016).
49. E. Spencer, M. Kiran, W. Li, U. Ramamurty, N. Ross, and A. Cheetham: Pressure-induced bond rearrangement and reversible phase transformation in a metal–organic framework. *Angew. Chem., Int. Ed.* **53**, 5583 (2014).
50. E. Spencer, J. Zhao, N. Ross, M. Andrews, R. Surbella, and C. Cahill: The influence of pressure on the photoluminescence properties of a terbium-adipate framework. *J. Solid State Chem.* **202**, 99 (2013).
51. E. Spencer, N. Ross, R. Surbella, and C. Cahill: The influence of pressure on the structure of a 2D uranium(VI) carboxyphosphonoate compound. *J. Solid State Chem.* **218**, 1 (2014).
52. K. Heffernan, N. Ross, E. Spencer, and L. Boatner: The structural response of gadolinium phosphate to pressure. *J. Solid State Chem.* **241**, 180 (2016).
53. E. Spencer, N. Ross, and R. Angel: The high pressure behaviour of the 3D copper carbonate framework $\{[Cu(CO_3)_2](CH_6N_3)_2\}_n$. *J. Mater. Chem.* **22**, 2074 (2012).
54. E. Spencer, V. Soghomonian, and N. Ross: Gallium arsenate dihydrate under pressure: Elastic properties, compression mechanism, and hydrogen bonding. *Inorg. Chem.* **54**, 7548 (2015).
55. M. Wojdyr: Fityk: A general-purpose peak fitting program. *J. Appl. Crystallogr.* **43**(5), 1126 (2010).
56. J. Rodriguez-Carvajal: FullProf Suite (LLB Sacley and LCSIM Rennes, France, 2003).
57. F. Birch: Finite elastic strain of cubic crystals. *Phys. Rev.* **71**, 809 (1947).
58. R. Angel, M. Alvaro, and J. Gonzalez-Platas: EosFit7c and a Fortran module (library) for equation of state calculations. *Z. Kristallogr.–Cryst. Mater.* **229**, 405 (2014).
59. B. McGrail, G. Sigmon, L. Jouffret, C. Andrews, and P. Burns: Raman spectroscopic and ESI-MS characterization of uranyl peroxide cage clusters. *Inorg. Chem.* **53**, 1562 (2014).
60. R. Haddon, L. Brus, and K. Raghavachari: Electronic structure and bonding in icosahedral C_{60}. *Chem. Phys. Lett.* **125**, 459 (1986).
61. J. Martin, S. Goettler, N. Fossé, and L. Iton: Designing intermediate-range order in amorphous materials. *Nature* **419**, 381 (2002).
62. X. Roy, C. Lee, A. Crowther, C. Schenck, T. Besara, R. Lalancette, T. Siegrist, P. Stephens, L. Brus, P. Kim, and M. Steigerwald: Nanoscale atoms in solid-state chemistry. *Science* **341**, 157 (2013).

Supplementary Material

To view supplementary material for this article, please visit https://doi.org/10.1557/jmr.2017.301.

https://doi.org/10.1557/jmr.2017.301 Published online by Cambridge University Press